Ion-pre intercalation of hydrated vanadium oxide cathode by K+ and its performance in Lithium-ion Battery

Di Huang

A thesis

submitted in partial fulfillment of the

requirements for the degree of

Master of Science

University of Washington

2022

Committee:

Guozhong Cao

Bruce Hinds

Program Authorized to Offer Degree:

Materials Science and Engineering

University of Washington

Abstract

Ion-pre intercalation of hydrated vanadium oxide cathode by K+ and its performance in Lithium-ion Battery

Di Huang

Chair of the Supervisory Committee:

Guozhong Cao

Department of Materials Science and Engineering

Layered hydrated vanadium oxides have a high theoretical capacity and low cost. Although its performance in lithium batteries has not yet been documented, it has promising futures in cathode materials for lithium-ion batteries. This paper describes a technique to produce distinctive hydrated vanadates by adding K+ to hydrated vanadium pentoxide (V2O5 nH2O, VOH). A new VOH phase with quicker ion diffusion kinetics and initial capacity is created when K+ is added. Its longer-term cycle stability still has to be enhanced, though. This work primarily documents the performance and structural modifications made to VOH after K+ integration. KVOH outperforms other batteries by displaying an impressive capacity of 316 mAh g1 at 0.2C and maintaining 227 138mAh g1 at 5C. While VOH showed a capacity of 157mAh/g at 0.2C and 38mAh/g at 5C.

1. Introduction

As the world is facing serious climate damage and resource depletion problems, under this trend, vigorously promoting new energy and renewable energy (such as wind energy, tidal energy, etc.) has become a new development direction. The growth and evolution of contemporary industry have also brought attention to the significance of creating a sustainable and environmentally friendly economy. According to the World Energy Statistical Yearbook, faster economic activity will cause global energy consumption to rise by 5.8 percent in 2021, surpassing pre-pandemic levels and increasing by 1.3 percent from 2019. Among them, fossil fuels accounted for 82% of primary energy use, compared with 83% in 2019 and 85% five years ago. Furthermore, the burning of fossil fuels will remain the world's largest energy consumer in the near future. Total world energy demand is expected to increase to 17,651 Mtoe by 2040, of which renewable energy accounts for only 20%. However, the widespread use of fossil fuels worldwide releases large amounts of carbon dioxide and other greenhouse gases (GHGs), leading to further global warming. Global carbon dioxide emissions from energy combustion and industrial processes will increase by 6% year-on-year to 36.3 billion tons in 2021. To address the energy and environmental issues associated with the burning of non-renewable fossil fuels, new energy and sustainable development approaches are urgently needed. Accelerating the development of new energy in the power and transportation industries is considered the most promising solution. However, due to the

bottleneck of technological development, the energy storage and utilization rate of this type of new energy are still relatively low and cannot be well utilized. Therefore, it is necessary to vigorously develop targeted advanced energy storage devices to improve energy utilization. At present, lithium-ion batteries are the most widely used and efficient electrochemical energy storage devices.

Lithium-ion batteries have achieved remarkable results so far. Due to its superior durability and lighter size than energy storage devices such as lead-acid batteries, it is increasingly used in new energy electric vehicles, personal electronics, mobile storage, etc. It is the most widely used battery Chemical energy storage technology. However, with the continuous changes in economic and industrial needs, lithium-ion batteries are currently plagued by problems such as low energy density, poor safety performance, and high package cost, which have greatly affected the current new energy vehicles and even the whole world. development of the industry[1]. As the core component to control the energy density and cost of lithium-ion batteries, cathode materials have become the focus of research in the current global lithium-ion battery field. Therefore, it is imperative to research a new generation of battery cathode/anode materials that have high specific energy, are more environmentally friendly, and have better cycle, environmental protection, and safety performance.

LIBs are primarily made up of positive electrode, negative electrode, electrolyte, separator, current collector, and battery shell in the current, relatively mature LIBs construction. Among them, the negative electrode is typically a widely used graphite that can intercalate lithium, and the positive electrode is a lithium-containing oxide (such $LiCO_2$, $LiFePO_4$, $LiMn_2O_4$, etc).[2] The separator successfully prevents contact between the positive and negative electrodes, so preventing the development of short circuits, and the current collector also acts as a channel for the intake and outflow of electrons. The electrolyte acts as a medium for lithium-ion transmission. The specific working principle of LIBs is shown in Figure 1.

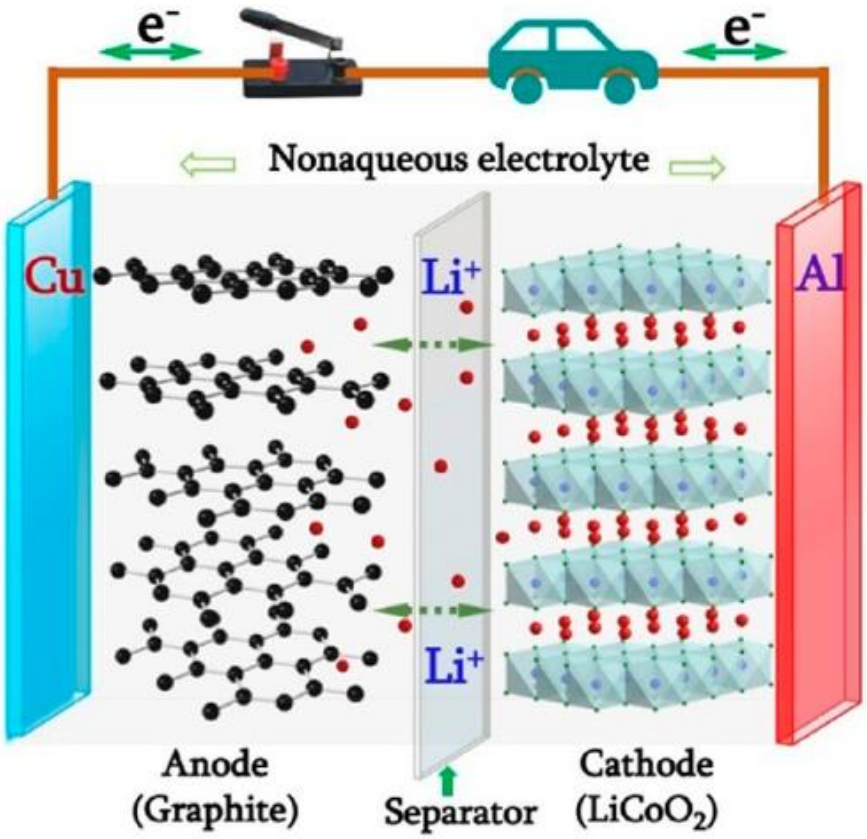

Figure 1. The charging and discharging process of lithium-ion batteries

When the LIBs are charged, the current of the charging power source will flow to the positive electrode of the LIBs, that is, electrons will flow from the positive electrode to the negative electrode in the external circuit so that under the action of the external electric field, and also to maintain charge conservation (or electrical neutrality), lithium ions will flow in the battery. The inner part is released from the positive electrode and moves to the negative electrode through the separator with the help of the electrolyte, and will eventually be embedded between the graphite negative electrode layers, thus realizing the storage of electric energy. As shown in Figure 1; when the LIBs are discharged, the lithium ions will move from the negative electrode to the positive electrode and re-insert into the positive electrode, and in order to maintain charge conservation, the electrons will flow out of the battery through the current collector and from the negative electrode in the external circuit. Flow to the positive electrode, that is, the current flows from the positive electrode to the negative electrode, thus realizing the release of electric energy, as shown in Figure 1. With the repeated charging and discharging of LIBs, lithium ions move back and forth between positive and negative inside the battery, so this working process of LIBs is also vividly called the "rocking chair" mechanism. The working theory of the aforementioned LIBs makes it clear that the electrode (positive and negative electrode) materials are the essential component of LIBs, and that the electrochemical performance of the battery, including its energy density, power

density, and cycle life, is directly influenced by the quality of the electrode material.[3]

The anode material is an important part of LIBs, and it needs to meet the following requirements: 1. the storage capacity of lithium is high; 2. the resistance of lithium ions to move between the interface of the electrode and the electrolyte is small, and the diffusion in the solid phase is small. The coefficient is large, so as to ensure the rapid intercalation and deintercalation of lithium ions between the electrodes; 3. High electronic conductivity; 4. The electrode material does not react with the electrolyte, and the lithium ions have a stable state in the electrodes; 5. Materials The volume changes little during the charging and discharging process; 6. The price is cheap, non-toxic and non-polluting. The earliest anode material used in LIBs is lithium metal, which not only has the advantage of high theoretical specific capacity (3860 mAh/g)[4], but also has the lowest standard potential compared to other anode materials, so it can make the battery have relatively maximum output. voltage, and thus has the relatively highest energy density. However, LIBs with lithium metal as the anode has a great potential safety hazard. The reason is that lithium ions will undergo non-uniform nucleation and precipitation on the surface of lithium metal, and even form lithium dendrites, thereby piercing the diaphragm, causing short circuit and explosion.In order to solve the above-mentioned problem of lithium dendrites, scientists have developed LIBs with graphite as the negative

electrode. For example, the first commercial LIBs launched by SONY in 1991 used graphite as the negative electrode. Graphite has the characteristics of good conductivity, low lithium intercalation potential, small volume change, good cyclability, and sufficient resources, and lithium ions can be very well de-intercalated and transported between layers of graphite (interlayer spacing of 0.335 nm). LiC_6 is formed when lithium ions are intercalated between the graphite layers, resulting in a theoretical specific capacity of 372 mAh/g[3][2]. Today, graphite is still the most mature and widely used anode material for LIBs. However, with the continuous development of new energy storage applications such as electric vehicles, higher requirements are also placed on the energy density of LIBs, resulting in that the theoretical specific capacity provided by graphite has gradually been unable to meet the requirements of such high energy density. On the other hand, the discharge voltage of graphite (about 0.1 V) is low, which will cause a high degree of decomposition of the electrolyte, and there are also potential safety hazards, especially when high energy density is required. Therefore, the research on negative electrodes has never stopped.

Positive electrode materials usually have specific capacities that are significantly lower than negative electrode materials. The theoretical specific capacity of $LiCoO_2$ in the positive electrode material used in the LIBs that Sony commercialized in 1991, for example, is only -140 mAh/g. The creation of LIBs cathode materials with greater capacity is therefore of the utmost importance.

Therefore, the cathode material has emerged as the key to controlling the ongoing development of LIBs' performance. There are several different cathode materials available for LIBs. Transition metal (TM) intercalation complexes make up the majority of the materials being studied at the moment that have showed some promise. They can be broadly categorized into three groups based on their distinct structures: compounds with a spinel structure, polyanionic compounds, and layered transition metal oxides.

Vanadium is a very abundant element in the earth's crust and has been widely studied due to its compounds with multiple oxidation states (II-V), abundant crystal structures, and high theoretical capacities. However, vanadium-based materials also suffer from a series of problems, such as intrinsic electron The low electrical conductivity and large volume change during cycling lead to poor rate performance and rapid capacity fading. In addition, complex and dangerous synthesis methods also limit their further development in the field of Li-ion batteries. To better understand the working mechanism of vanadium oxide electrodes and improve the electrochemical performance of vanadium oxides, the current research mainly focus on control the microstructure and electronic structure of vanadium-based materials, to optimize their electrochemical properties, and to reveal the structure at the same time. The structure-activity relationship between electrochemical performance and vanadium-based materials will further promote the development of vanadium-based materials in

the field of ionic batteries and other new energy storage and conversion fields.[6]

Vanadium pentoxide has emerged as one of the most promising cathode materials and has been widely researched for LIBs due to its high energy density, low cost, simple preparation, plentiful sources, and adequate safety features. In particular, V_2O_5 is a very promising cathode material for next-generation LIBs due to its layered structure and theoretical capacity of 294 mAh/g with the de/intercalation of two Li^+, which is significantly higher than that of other cathode materials that are frequently used.[6]

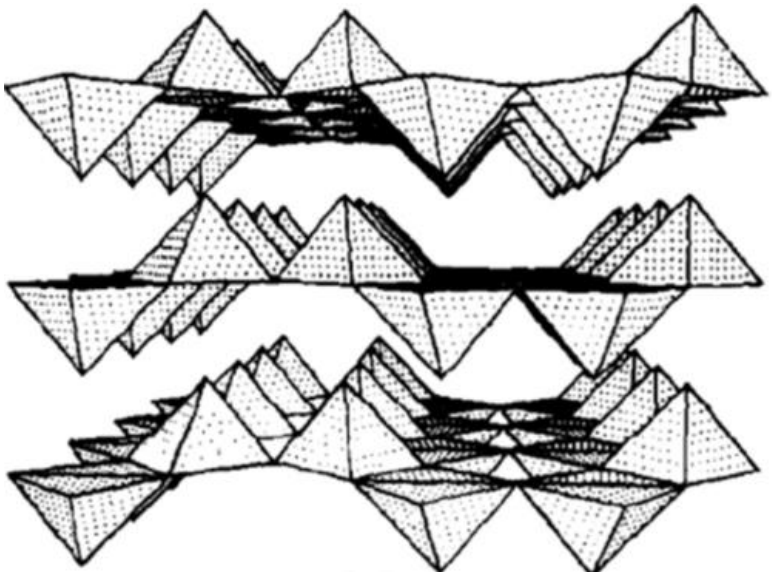

Figure 2. The structure of V_2O_5[7]

However, the practical reversible capacity of crystalline V_2O_5 is substantially smaller since such a deep discharge/charge depth ($x > 1$ in $LixV_2O_5$) would result in a large irreversible capacity lost at the first cycle as well as rapid

capacity decay in subsequent cycles. Hydrated vanadium pentoxide ($V_2O_5.xH_2O$) with expanded interlayer distance (from 8.75 Å to 12 Å) can promise both high overall diffusion coefficient and low volume expansion during lithium intercalation, demonstrating higher reversible capacity, enhanced rate capability, and better cycle stability compared to crystalline V2O5. However, because of its confusing chemical composition, indeterminate crystallographic structure, and sensitivity to moisture, hydrated vanadium pentoxide is difficult to handle as an electrode material. In actuality, it is hydrated vanadium oxide with a mixed valence of V^{4+}/V^{5+} since some reduction of V^{5+} happens during the synthesis's sol-gel process. The mix-valence nature promises variable conversion options to various vanadium oxides with higher or lower valence state. Despite of its quick capacity fading, the hydrated vanadium oxide δ-V_2O_5·nH2O is particularly promising due to its expanded interlayer spacing (∼12 Å), mixed valence states (V^{5+} and V^{4+}), and the fast ion-exchange capability.

Ion-preintercalation is the most successful and facile strategies to stabilize the layered structure by far. Various of ion species have been explored to adjust the interlayer spacing and chemical makeup of hydrated vanadium pentoxide. The metal ion-preintercalated vanadium oxides (MVOH) have greater specific capacities and improved capacity retention when compared to the pure V_2O_5-nH_2O phase (VOH). The present work investigates the fabrication and the

detailed structural and electrochemical characterization of K+ preintercalated hydrated vanadate (KVOH). It is a new phase compared to hydrated vanadium pentoxide (V2O5·nH2O, VOH), with higher capacity and better kinetic.[6]

2. Experimental Section

Material synthesis: All chemicals were obtained from Fisher Scientific Inc or Sigma-Aldrich Inc without further purification. In a typical experiment, 0.364 mg of V_2O_5 (Sigma-Aldrich) was dissolved into 50 mL of DI water with adding 2 mL of H_2O_2 (30%, Fisher Scientific). 0.087 mg of K_2SO_4 (Sigma-Aldrich) with the molar ratio to V_2O_5 of 1:4 was dissolved into 30 mL of DI water. Then these two solutions were mixed under magnetic stirring for 0.5 h and transferred into 100 mL of Teflon lined stainless steel autoclave under 120 ˚C for 6 h. The obtained precipitates were washed by DI water and ethanol for three times and dried in an oven at 60 ˚C for 20 h to remove solvent and obtain green powder, named as KVOH. Hydrated vanadium oxide (VOH) was prepared in the same conditions just without adding K_2SO_4.

Characterizations: X-ray diffraction (XRD) was used to identify the compositions and structures of the products using Bruker D8 Discover X-ray diffractometer with an ImS 2-D detection system (50 kV, 1000 mA). The

microstructures of the samples were observed using a scanning electron microscope (Apreo-S LoVac) with an Energy-dispersive X-ray spectrometer (EDS). X-ray photoelectron spectrum (XPS) was taken on a Thermo ESCALAB 250XiX spectrometer with monochromatized Al Kα X-ray (hν ¼ 1486.6eV). Thermogravimetric analysis (TA Instruments Q50 thermogravimetric analyzer) was employed to investigate the water content.

Electrochemical Measurements: The cathode electrodes were fabricated by mixing 80% of active materials, 10% of conductive carbon and 10% of polyvinylidene fluoride (PVDF) binder dispersed in N Methyl-2-Pyrrolidone (NMP) solvent and the slurry was dripped on Aluminum foil. The prepared electrodes were dried in a vacuum oven under 120 ˚C for 12 h to remove residual solvent. The lithium ion batteries (LIBs) were assembled in CR2032 coin cells in an argon atmosphere glove box, with as-prepared materials as the cathode, Lithium metal chip as the anode, Polypropylene (PP) monolayer film as the separator and 1.0 M LiPF6 in EC/DMC=50/50 (v/v)(battery grade) as the electrolyte. The redox behavior of LIBs was conducted by cyclic voltammogram (CV) on Solartron electrochemical station (SI 1287) conjectured with an electrochemical impedance spectroscope (EIS, SI 1260). The EIS spectra were obtained at the frequency range of 100 to 0.01 Hz. The galvanostatic charge/discharge (GCD) was carried out from 2 to 4 V on Neware tester (CT-4008). The rate performance, the energy efficiency, the energy density and

power density were calculated according to GCD results at various current densities based on active mass of cathode materials. The cycling stability was evaluated at the current density of 0.5C for 200 cycles. Batteries were fully discharged to 2V and then charged to 4V to achieve one cycle, then this process was repeated for 200 cycles.

3. Result and Discussion

KVOH was prepared by a facile one-step hydrothermal method without further annealing. Figure,3a exhibits microspheres of KVOH consisting of numerous nanorods with the diameter around 10μm. Energy-dispersive X-ray spectrometer (EDS) elemental mapping images (Fig. 3b) reveal the homogenous distribution of the K, V, and O in the KVOH nanoribbons, confirming the successful introduction of K-ions in the VOH. X-ray diffraction (XRD) is conducted to investigate the crystal structural information. The XRD patterns of KVOH and VOH are displayed in Fig. 3c.

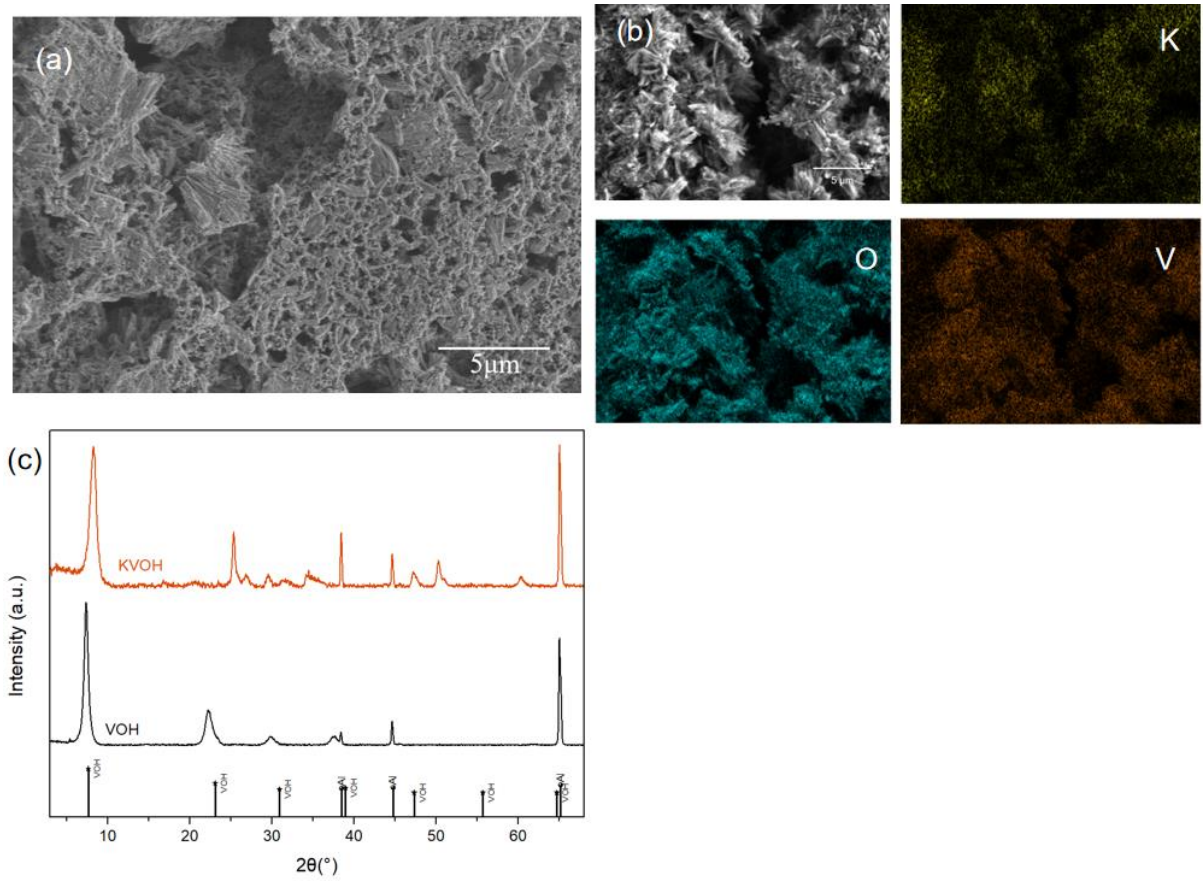

Figure 3. SEM and EDS Spectrum of pristine KVOH

XRD patterns in Fig. 3c provide more information about the crystalline structure of samples. KVOH performs a typical bilayer structure similar to $V_2O_5 \cdot 1.6H_2O$ (JCPDS #40–1296), two samples' strong (00l) diffraction peaks reveal a typical layered structure along the c-axis, composed of $[VO_5]$ and $[VO_6]$ polyhedron and water molecules between layers. For KVOH, it demonstrates a unique XRD pattern, different from that reported in the literature with K+ incorporated into the structure, which the standard XRD pattern of KVOH could not be provided

based on current database. When compared to VOH (2θ= 7°), KVOH's (001) peak shifts toward a greater degree of 8.2°. Through the Bragg's equation,

$$2dsin\theta = n\lambda$$

it can be calculated that, KVOH exhibits a contracted lattice spacing of 10.6 Å, smaller than 12.0 Å of VOH, an indication of structure shrinkage after K+ introduction, which may be due to the strong interaction of K+ and O- to form a K-O bond that reduces the lattice spacing.[8][9]

The samples' thermal stability and degree of hydration (n in -KxV2O5nH2O) were evaluated using simultaneous thermogravimetry analysis (TGA).

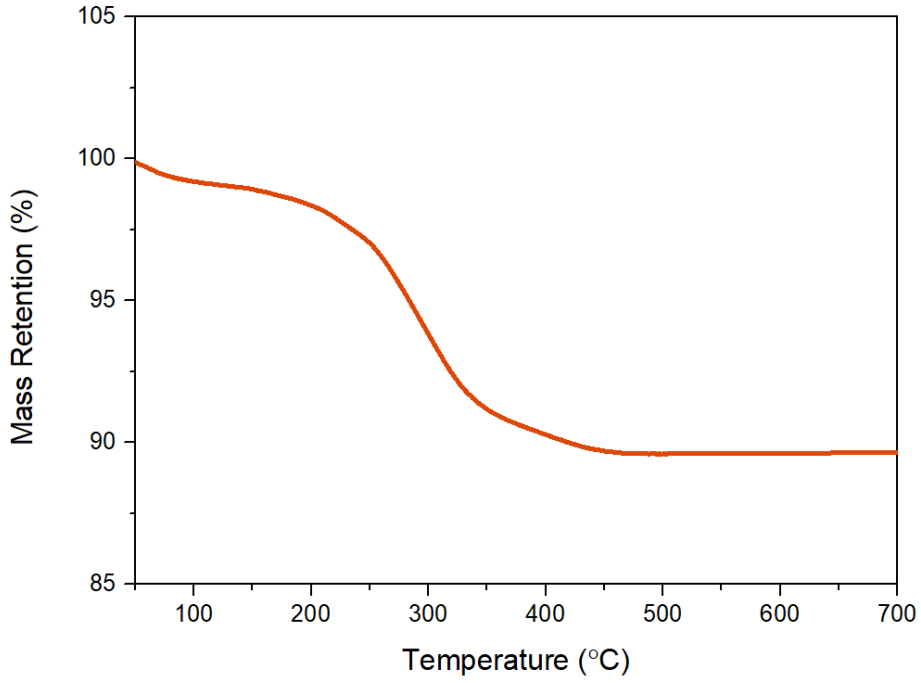

Figure 4. TGA of KVOH

Weight losses with rising temperature are depicted in Fig. 4 and are attributed to two different types of interlayer water in V_2O_5-nH_2O. The amount of physically

adsorbed and weakly bound water, which leaves at 120 °C, is dictated by the water pressure in the surrounding environment. The water that is chemically and tightly bound to the vanadium oxide network separates from the other kind around 250 °C.

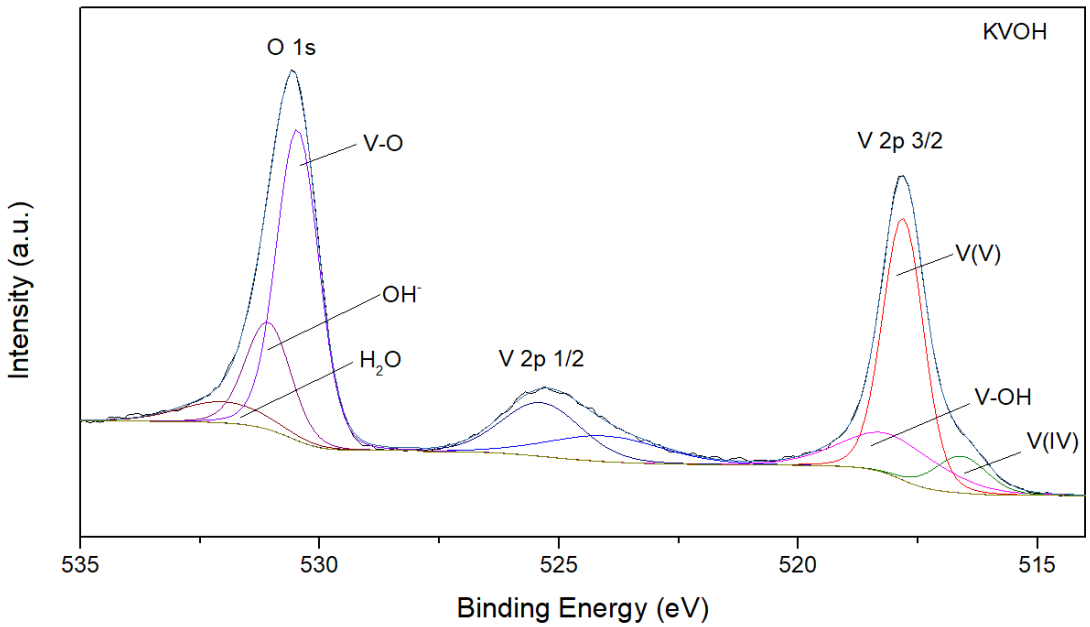

Figure 5. XPS spectrum of KVOH

The embedment of K^+ into the lattice of KVOH is revealed by the X-ray photoelectron spectroscopy (XPS) survey spectrum (Fig. 5), where a distinct K 2s signal is found at 374.9eV. The V 2p3/2 spectra show that KVOH samples have a mixture of V^{5+} and V4+ valence states. The peak associated with the oxidation state of V^{5+} was centered at a higher binding energy of 517.8 eV, while V^{4+}'s peak was associated with a lower binding energy of 516.6 eV[10]. The average oxidation state of KVOH is determined to be $V^{4.72+}$ based on the 1:2.6 molar ratio of V^{4+} to V^{5+} in KVOH.

The Li-ion storage performance of KVOH and the role of preintercalated K+ ions were evaluated by assembling CR 2032 coin cells using 1 M LiPF6 as the electrolyte and Li metal chip as the anode. Fig. 6(a) shows the initial three cyclic voltammetry (CV) profiles of Li+/KVOH cells tested within the voltage range of 2~4 V at a scan rate of 0.1 mV/s. Two pairs of well-defined redox peaks are observed at 2.41V/2.74V and 2.76V/2.98V, which are ascribed to the redox reactions between V^{5+}/V^{4+} and V^{4+}/V^{3+} pairs, respectively.

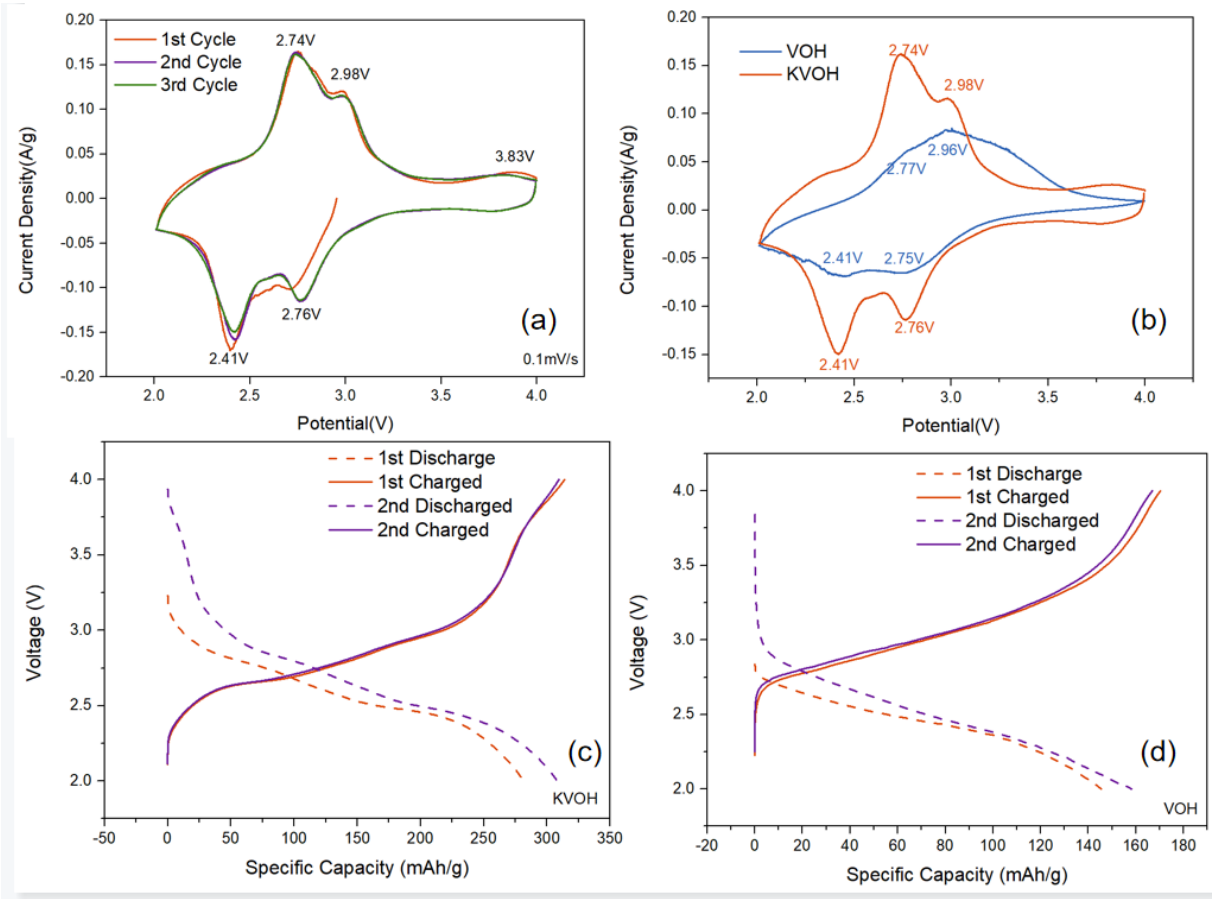

Figure 6. (a) The initial three cycles of CV curves for KVOH at a scan rate of 0.1 mV/s. (b) CV curves of KVOH and VOH at 0.1 mV/s. (c) The 1st and 2nd galvanostatic charge/discharge curves of KVOH at a current density of 0.2C. (d) The 1st and 2nd galvanostatic charge/discharge curves of VOH at a current density of 0.2C.

The KVOH's first three cycles' well-overlapping CV patterns point to a highly reversible electrochemical Li+ insertion/extraction process. Fig. 6b displays the third cycle CV curves for KVOH and VOH at scan rate of 0.1mV/s for comparison's sake. There are also two pairs of redox peaks of VOH are observed at 2.41V/2.77V and 2.75V/2.96V. They both contain peaks at the same locations and comparable forms, which suggests that both materials experience the same redox processes during the electrochemical Li^+ ion intercalation/deintercalation. The two samples differ in that KVOH has a larger current response and a larger integrated area of CV curves than VOH, which suggests that KVOH has a greater capacity. As opposed to being two separate peaks as in KVOH, the two peaks are combined to form a single, broad redox plateau, suggesting that the intercalation of K ions enhances the electrochemical activity of VOH.[13][18]

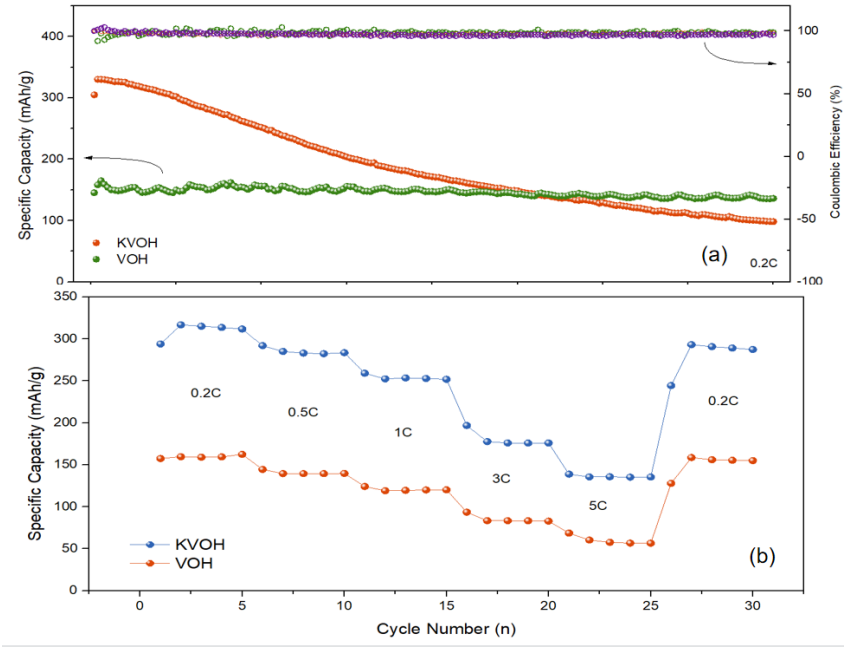

Figure 7. (a) Long-term cycling stability of KVOH and VOH at 0.2C. (b) Rate capability of KVOH and VOH.

In Fig. 7b, the rate responses of KVOH and VOH are contrasted. At 0.2C, 0.5C, 1C, 3C, and 5C, K pre-intercalated hydrated vanadium pentoxide has discharge capacities of 316, 291, 258, 196, and 138 mA h/g, respectively. A reversible capacity of 138 mA h/g is delivered when the current density rises to 5C, resulting in a capacity retention of 43%. (with respect to the capacity at 0.2C). A reversible capacity of 244 mA h/g can be restored when the rate drops to 0.2C, demonstrating KVOH's structural stability and electrochemical reversibility. In contrast, the capacity of the VOH cathode is less than that of KVOH at all current densities. The discharge capacities of VOH at 0.2C, 0.5C 1C, 3C, and 5C are 157, 144, 124, 93, and 68 mA h/g, respectively and it has 43% capacity retention as well, when the current density increases from 0.2C to 5C. A reversible capacity of 127 mA h/g can be restored when the rate drops to 0.2C show little difference with KVOH. The long-term cycling performance of the Li/KVOH and VOH cells were evaluated at current density of 0.2C (Fig. 7a). After the first 130 cycles, the discharge capacity of KVOH had gradually fallen to a level below that of VOH. KVOH only has a 98mA h/g specific capacity left after 200 cycles (31 percent capacity retention). However, the discharge capacity of VOH is relatively stable for all 200 cycles, and after 200 cycles, it maintains a specific discharge capacity of 136 mA h/g (capacity retention rate of 96%), which is much higher than that of KVOH.

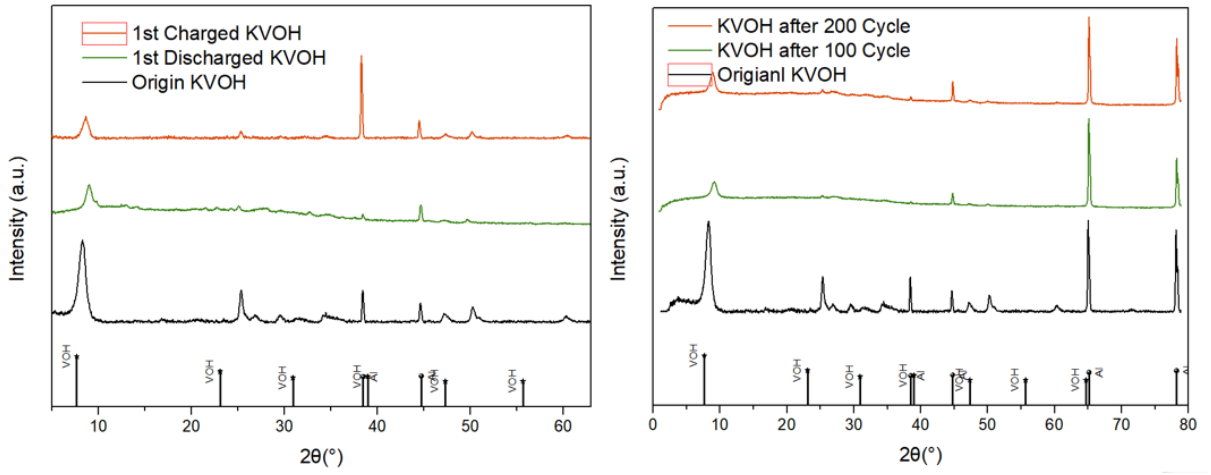

Figure 8. Ex-situ XRD patterns of KVOH electrodes at the pristine, fully discharged and charged, after100/200 cycle states

Ex-situ XRD was used to explore into how the structure of KVOH altered throughout the Li+ ion intercalation and deintercalation processes. After first charging and discharging, KVOH's ex-situ XRD patterns are displayed in fig 8. After being discharged to 2V, the (001) peak changes from its initial state's lower degree (8.28°) to a higher degree (8.94°), which is consistent with an interlayer compression caused by Li+ ion insertion. In the wake of the subsequent charging to 4V, the (001) peak returns to its original region associated with Li+ extraction. The shifting mechanisms of the (003), (004), and (005) peaks are also comparable when cycled, proving that Li^+ intercalation/deintercalation in KVOH is highly reversible. The fact that KVOH displays nearly identical characteristic peaks to those of VOH suggests that the bilayered structure of VOH has been well conserved following the addition of Li^+ cations. Additionally, it is demonstrated that cycling preserves the KVOH's original layered structure, indicating the structure's structural stability. After

100/200 cycles, although the characteristic peaks of VOH can still be observed, its diffraction intensity is greatly reduced, indicating the decrease of particle size of KVOH and the overall crystallinity after cycling.

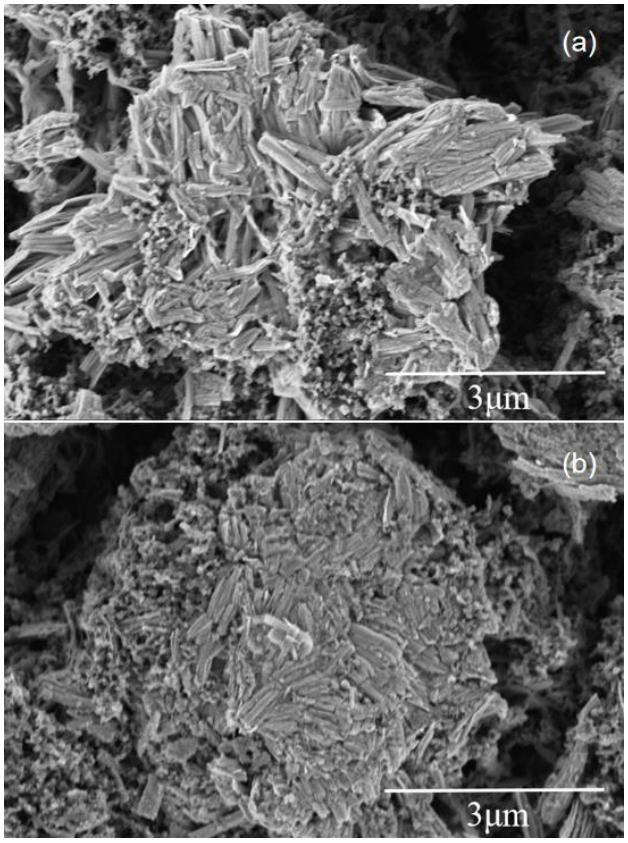

Figure 9. SEM images of (a) KVOH after 50 cycles. (b)KVOH after 200 cycles.

The SEM image of KVOH following 50/200 cycles is shown in Figure 9. The figure shows that the original nanorod length has been decreased from 3 μm to roughly less than 1μm. It demonstrates that after 200 cycles, the average particle size of KVOH has decreased. This matches the XRD pattern following 100 or 200 cycles. The typical VOH peaks are still visible, but the diffraction strength is much diminished.

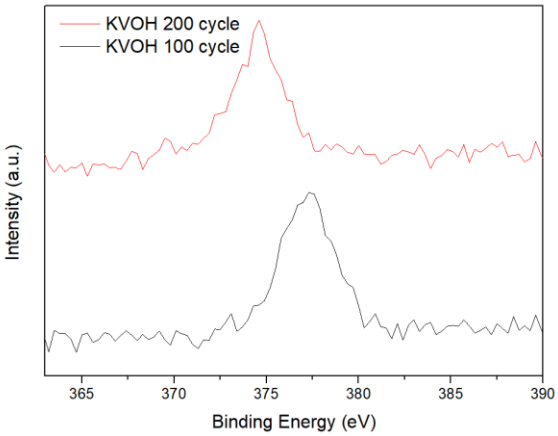

Figure 10. K 2s XPS spectra

Figure 10 shows the K 2s-XPS spectra after 100/200 cycles. Despite the KVOH particle size decreasing and the crystallinity deteriorating, the intercalated K element is still hydrated with potassium pentoxide after 100/200 cycles. It matches the findings of the XRD pattern in vanadium.

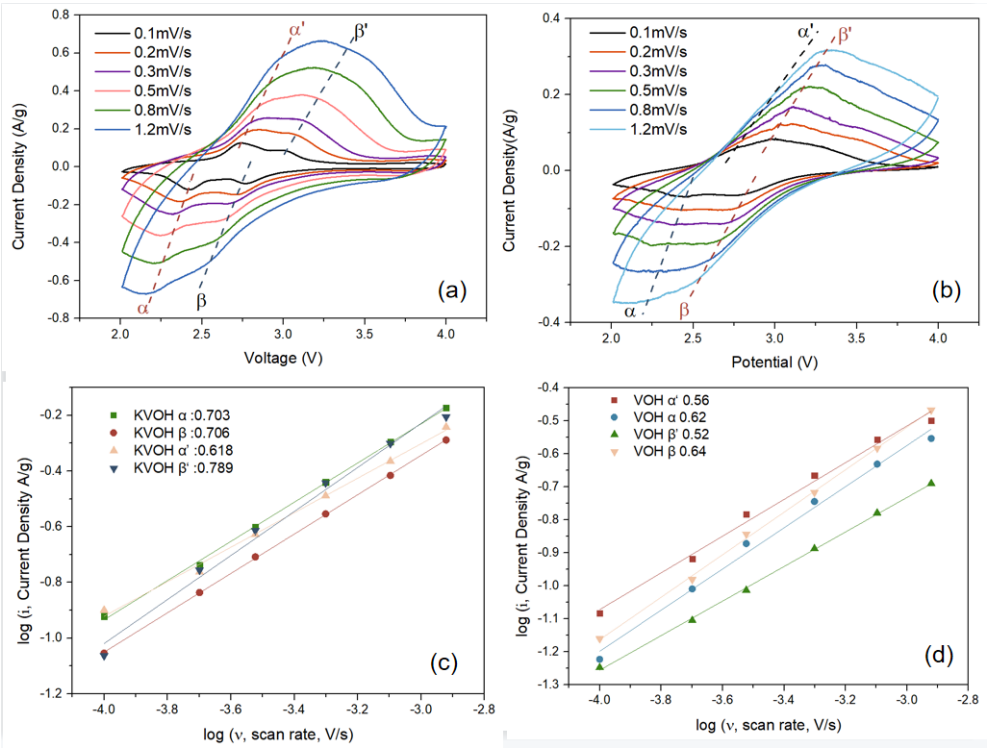

Figure 11. (a) CV curves of the Li/KVOH cell at various scan rates. (b) CV curves of the Li/VOH cell at various scan rates. (c) b-values of redox peaks in CV curves of KVOH. (c) b-values of redox peaks in CV curves of VOH.

In order to investigate the kinetics of the electrochemical process, CV analysis is performed at various scan rates. The reduction and oxidation peaks move to lower and higher voltages, respectively, when the scan rate rises from 0.1 to 1.2 mV/s because of the expanded polarization, as shown in the fig 11a and fig 11b. However, the stable forms of CV curves with higher scan speeds show that Li intercalation and deintercalation in KVOH are simple and reversible without crystallographic phase change. Theoretically, the relationship between the response current and the scan rate can be described by the following equation.

$$\boldsymbol{i_p = av^b}$$

where variables a and b can be changed. A process that is surface-controlled has a b = 1 while a process that is diffusion-controlled has a b = 0.5. Different KVOH redox peaks have b values ranging from 0.5 to 1(fig 11c), which suggests a hybrid diffusion-surface controlled mechanism. Greater contributions from a surface-controlled process for KVOH during charge/discharge cycles are revealed by KVOH having higher b values than VOH.

3. Conclusion and Future Work

Overall, K-intercalated VOH was successfully synthesized by a one-step hydrothermal method. After K-intercalation, the interlayer spacing of VOH shrinks from the original 12 Å to 10.6 Å. At the same time, the interlayer spacing will further shrink when Li ions are inserted, but the interlayer spacing will expand with the extraction of Li ions. The insertion of K ions increased the initial capacity of VOH from 157mAh/g to 316mAh/g. Meanwhile, the insertion of K enhances the reversibility and kinetics of the electrode reaction of VOH. But as the number of battery cycles increases, the capacity of K intercalated VOH decays rapidly and is lower than the VOH without K intercalation after 130 cycles. Therefore, K insertion successfully improves the kinetic performance and capacity of VOH, its cycling stability is much lower than expected. Further research is still needed to improve its cycling stability.

Future work:

1. Conduct more research on the causes of the hydrated vanadium pentoxide's rapid capacity decline caused by K ion intercalation, including testing the KVOH pole piece after 50, 100, 150, and 200 cycles, examining changes to its structure and chemical bonds, and searching for patterns.
2. Look for methods, such as intercalation or coating modification of different ions, to enhance K pre-intercalation of hydrated vanadium pentoxide.

3. Examine how VOH intercalated with various alkali metal ions performs in lithium batteries, contrast the rules, and identify more optimal intercalation ions.

References

[1]. Mahmud, Rahman, M., Kamruzzaman, M., Ali, M. O., Emon, M. S. A., Khatun, H., & Ali, M. R. (2022). Recent advances in lithium-ion battery materials for improved electrochemical performance: A review. Results in Engineering, 15, 100472–. https://doi.org/10.1016/j.rineng.2022.100472

[2]. Nzereogu, Omah, A. D., Ezema, F. I., Iwuoha, E. I., & Nwanya, A. C. (2022). Anode materials for lithium-ion batteries: A review. Applied Surface Science Advances, 9, 100233–. https://doi.org/10.1016/j.apsadv.2022.100233

[3]. Cao, Qiao, Y., Jia, M., He, P., & Zhou, H. (2022). Ion‐Exchange: A Promising Strategy to Design Li‐Rich and Li‐Excess Layered Cathode Materials for Li‐Ion Batteries. Advanced Energy Materials, 12(4), 2003972‐n/a. https://doi.org/10.1002/aenm.202003972

[4]. Manthiram. (2017). An Outlook on Lithium Ion Battery Technology. ACS Central Science, 3(10), 1063–1069. https://doi.org/10.1021/acscentsci.7b00288

[5]. Tian, Liu, C., Zheng, J., Jia, X., Jahrman, E. P., Seidler, G. T., Long, D., Atif, M., Alsalhi, M., & Cao, G. (2020). Structural engineering of hydrated vanadium oxide cathode by K+ incorporation for high-capacity and long-cycling aqueous zinc ion batteries. Energy Storage Materials, 29, 9–16. https://doi.org/10.1016/j.ensm.2020.03.024

[6]. Jia, Liu, C., Neale, Z. G., Yang, J., & Cao, G. (2020). Active Materials for Aqueous Zinc Ion Batteries: Synthesis, Crystal Structure, Morphology, and Electrochemistry. Chemical Reviews, 120(15), 7795–7866. https://doi.org/10.1021/acs.chemrev.9b00628

[7]. Yao, Li, Y., Masse, R. C., Uchaker, E., & Cao, G. (2018). Revitalized interest in vanadium pentoxide as cathode material for lithium-ion batteries and beyond. ENERGY STORAGE MATERIALS, 11, 205–259. https://doi.org/10.1016/j.ensm.2017.10.014

[8]. Bondarenka, Jasulaitienė, V., Sereika, R., & Stirkė, A. (2014). Sol–gel synthesis and XPS study of vanadium pentoxide xerogels intercalated with glucose. Journal of Sol-Gel Science and Technology, 71(3), 385–390. https://doi.org/10.1007/s10971-014-3385-6

[9]. Zhong, Huang, J., Liang, S., Liu, J., Li, Y., Cai, G., Jiang, Y., & Liu, J. (2020). New Prelithiated V2O5 Superstructure for Lithium-Ion Batteries with Long Cycle Life and High Power. ACS Energy Letters, 5(1), 31–38. https://doi.org/10.1021/acsenergylett.9b02048

[10]. Rui, Zhu, J., Liu, W., Tan, H., Sim, D., Xu, C., Zhang, H., Ma, J., Hng, H. H., Lim, T. M., & Yan, Q. (2011). Facile preparation of hydrated vanadium pentoxide nanobelts based bulky paper as flexible binder-free cathodes for high-performance lithium ion batteries. RSC Advances, 1(1), 117–122. https://doi.org/10.1039/c1ra00281c

[11]. Zhang, Yuan, X., Lu, T., Gong, Z., Pan, L., & Guo, S. (2021). Hydrated vanadium pentoxide/reduced graphene oxide composite cathode material for high-rate lithium ion

batteries. Journal of Colloid and Interface Science, 585, 347–354. https://doi.org/10.1016/j.jcis.2020.11.074

[12]. Moretti, & Passerini, S. (2016). Bilayered Nanostructured V2O5·nH2O for Metal Batteries. Advanced Energy Materials, 6(23). https://doi.org/10.1002/aenm.201600868

[13]. Etman, Inge, A. K., Jiaru, X., Younesi, R., Edström, K., & Sun, J. (2017). A Water Based Synthesis of Ultrathin Hydrated Vanadium Pentoxide Nanosheets for Lithium Battery Application: Free Standing Electrodes or Conventionally Casted Electrodes? Electrochimica Acta, 252, 254–260. https://doi.org/10.1016/j.electacta.2017.08.137

[14]. Passerini, Ressler, J., Le, D., Owens, B., & Smyrl, W. (1999). High rate electrodes of V2O5 aerogel. Electrochimica Acta, 44(13), 2209–2217. https://doi.org/10.1016/S0013-4686(98)00346-6

[15]. Zhang, Yuan, X., Lu, T., Gong, Z., Pan, L., & Guo, S. (2021). Hydrated vanadium pentoxide/reduced graphene oxide composite cathode material for high-rate lithium ion batteries. Journal of Colloid and Interface Science, 585, 347–354. https://doi.org/10.1016/j.jcis.2020.11.074

[16]. Mai, Xu, X., Xu, L., Han, C., & Luo, Y. (2011). Vanadium oxide nanowires for Li-ion batteries. Journal of Materials Research, 26(17), 2175–2185. https://doi.org/10.1557/jmr.2011.171

[17]. Li, He, P., Wang, Y., Hosono, E., & Zhou, H. (2011). High-surface vanadium oxides with large capacities for lithium-ion batteries: from hydrated aerogel to nanocrystalline

VO2(B), V6O13 and V2O5. Journal of Materials Chemistry, 21(29), 10999–11009. https://doi.org/10.1039/c1jm11523e

[18]. Pan, Liu, D., Zhou, X., Garcia, B. B., Liang, S., Liu, J., & Cao, G. (2010). Enhanced lithium-ion intercalation properties of coherent hydrous vanadium pentoxide–carbon cryogel nanocomposites. Journal of Power Sources, 195(12), 3893–3899. https://doi.org/10.1016/j.jpowsour.2009.12.120

[19]. Tian, Li, N., Xie, K., & Niu, C. (2019). Towards high energy-high power dendrite-free lithium metal batteries: The novel hydrated vanadium oxide/graphene ∥ silicon nitride/lithium system. Journal of Power Sources, 417, 14–20. https://doi.org/10.1016/j.jpowsour.2019.02.007

[20]. Sun, Yang, S.-B., Lv, L.-P., Lieberwirth, I., Zhang, L.-C., Ding, C.-X., & Chen, C.-H. (2013). A composite film of reduced graphene oxide modified vanadium oxide nanoribbons as a free standing cathode material for rechargeable lithium batteries. Journal of Power Sources, 241, 168–172. https://doi.org/10.1016/j.jpowsour.2013.04.093

[21]. Li, Chang, K.-H., & Hu, C.-C. (2010). A novel vanadium oxide deposit for the cathode of asymmetric lithium-ion supercapacitors. Electrochemistry Communications, 12(12), 1800–1803. https://doi.org/10.1016/j.elecom.2010.10.029

[22]. Park, So, S., & Hur, J. (2022). Carbon-free hydrated cobalt vanadium oxide as a promising anode for lithium-ion batteries. Applied Surface Science, 579, 152182–. https://doi.org/10.1016/j.apsusc.2021.152182